Wood Science and Technology (2024) 58:379–402
https://doi.org/10.1007/s00226-023-01526-x

ORIGINAL

Adhesion-related properties of silver birch (*Betula Pendula* Roth) wood as affected by hydrophilic extraction

Max Engelhardt[1] · **Hans Albert Gilg**[2] · **Klaus Richter**[1] · **Antoni Sanchez-Ferrer**[1]

Received: 4 October 2023 / Accepted: 19 December 2023 / Published online: 7 January 2024

Abstract

For the utilization of silver birch (*Betula pendula* Roth) in load-bearing engineered wood products (EWPs), reliable bonding in production is a prerequisite. The current knowledge regarding the bonding of birch in EWP applications is limited. Extractives are considered a general factor of attention when securing bonding quality. Thus, in this study, the effects of hydrophilic extractives on several adhesion-related bulk and surface properties of silver birch wood were studied, e.g., vapor sorption, swelling behavior, microstructure, wettability, and mechanical properties. The extraction procedure slightly affected vapor sorption causing a reduction in swelling pressure. The extraction also led to a lower Young's modulus, as seen by compression tests. Control experiments with vapor-treated specimens, however, indicated that the effects were originating from the water imbibition and not due to the removal of extractives per se. This was supported by X-ray diffraction results, which were similarly affected by both vapor and extraction treatment. Therefore, the results indicate that the hygric history of the specimens was affecting the wood due to plasticization, increasing mobility, and thereby likely allowing biopolymer reconfiguration and subsequent quenching during re-drying, even though surface-free energy and wettability were not considerably affected. The extent to which these changes appear permanently or temporarily remains an open research question.

✉ Max Engelhardt
engelhardt@hfm.tum.de

✉ Antoni Sanchez-Ferrer
sanchez@hfm.tum.de

Hans Albert Gilg
agilg@tum.de

Klaus Richter
richter@hfm.tum.de

[1] Chair of Wood Science, TUM School of Life Sciences, Technical University of Munich, Winzererstr. 45, 80797 Munich, Germany

[2] Department of Civil Geo and Environmental Engineering, TUM School of Engineering and Design, Technical University of Munich, Munich, Germany

Introduction

The birch species (*Betula* spp.) are regarded to have considerable potential to facilitate climate-smart forestry targets (*e.g.*, increase diversity in mixed-stand silviculture, quick reforestation after forest disturbances) and wood industry (Dubois et al. 2020) in northern and central Europe, where birch is native. Silver birch (*B. pendula*) has a widespread transcontinental distribution from North America and Eurasia's boreal to subtropical and temperate regions (Ashburner et al. 2013). It shows a sufficient tolerance regarding soil conditions and water availability (Roloff and Grundmann 2008). In terms of industrial use, it can generate competitive round wood yields, especially for rotary-cut veneers (Cakiroglu et al. 2019). While its wood does not possess high natural durability (Andersons et al. 2009; Grinins et al. 2021), the diffuse-porous hardwood has valuable mechanical properties regarding strength and stiffness (Schlotzhauer et al. 2017; Baumann et al. 2020; Senalik and Farber 2021), also under rolling shear loading (Ehrhart et al. 2015), which makes it a potential candidate for engineered wood products (EWPs) in structural building applications (Jeitler and Augustin 2016; Fleer 2019).

In engineered wood flooring (EWF), birch plywood is already an established core layer material (Bouffard et al. 2010). However, birch wood lacks extensive research on bondability in EWPs and their use in load-bearing constructions. Recent research focused on the factor of extractives on birch bonding and identified the influence of hydrophilic birch extractives on the adhesive properties, their curing behavior, and the resulting bond line performance (Engelhardt et al. 2023). With this study, the exploration of the role of hydrophilic birch wood extractives on structural bonding is extended to their potential of modifying the adherend's properties, *i.e.*, physical bulk and wood surface properties.

The water relations of the substrate are of general importance in wood bonding since most adhesives used are water-based and, when curing, water needs to be adsorbed by the substrate. On the other hand, water-free adhesives are mostly isocyanate-based reactive adhesives, which need to be given water from the substrate to cure. Therefore, the wood's moisture interaction characteristics are connected to the dynamic bonding process and it has been shown to be affected by extractives. Extractives can affect adsorption levels (Choong and Achmadi 1991; Hernández 2007) in the multilayer domain due to bulking effects (Wangaard and Granados 1967; Popper et al. 2006) or in the case of hydrophilic extractives (*e.g.*, simple sugars or glycosides) also the physisorption at lower RH levels (Zhou et al. 2016). The effects are specific to the chemical nature of the extractives occurring in a particular wood.

The extent and the resulting stresses of wood swelling or shrinking are relevant factors for reliable wood bonding (Hofferber et al. 2006; Frihart 2007) since EWPs are subject to changing environmental conditions during service life. Although some studies exist on the swelling behavior of birch wood (Kumar 1957; Noack et al. 1973; Giebeler 1983), whether the hydrophilic extraction treatment can affect the swelling properties is unknown.

Theoretically, low molecular mass extractives can act as plasticizers. On the other hand, reinforces the structure due to the bulking action by pore filling, as claimed by Grabner et al. (2005), where it was shown that the hydrophilic extraction of larch wood led to reduced transversal strength and modulus of elasticity. However, studies on the effect of extractive concentration or extraction treatments on basic mechanical wood properties are scarce and were not found for birch wood.

As one of the adhesion mechanisms, the molecular attraction due to the surface free energy of the substrate, which promotes wetting and bond line formation, has also been found to be affected by wood extraction, including water extraction (Nzokou and Kamdem 2004). However, mostly softwood species, such as spruce (Walinder and Gardner 2000) or pine (Tshabalala 1997; Liu et al. 1998), were studied in this regard.

Within this study, the moisture interactions, the hygroscopic swelling behavior, and mechanical stiffness shall be understood in terms of their sensitivity to a hydrophilic extraction treatment. Thus, it encompasses an experimental screening of bondability-related bulk properties, which were investigated as the water-based extraction treatment procedure possibly modifies them. These modifications can be due to the removal of the extractives per se but can also be concomitant effects due to the phase of high-water uptake (imbibition), the swelling of amorphous polymer domains in the wood, which might allow for relaxation and reconfiguration processes. Hence, additional control experiments on specimens using an alternative treatment—storage in close-to-saturated vapor conditions—should discern, whether water imbibition is responsible for those changes or the actual removal and consequent absence of extractives. The study further aims to understand, via X-ray diffraction (XRD) analysis, whether microstructural characteristics changes took place after treatments with water, which are in agreement with the observed effects. Finally, since an extraction results in an altered chemical composition of wood, the study additionally aims to characterize surface properties (*i.e.*, adhesive wettability, surface free energy, and surface acidity) of birch wood and identify whether they are subject to change due to the removal of hydrophilic extractives.

Experimental section

The study investigated silver birch wood (*Betula pendula* Roth), of which boards were used as raw material for various specimens. Unless stated otherwise, sapwood (no discoloration) from Lieska (Finland) and Eberswalde (Germany) regions was used to produce the various specimens in equal amounts for the experiments.

Specimen preparation and treatment

The green sawn boards were kiln-dried to a final moisture content of 10–11%. The boards were stored after drying in constant conditions of 20 °C and 65% RH. This state is further referred to as the untreated state, *i.e.*, pristine condition. Small-scale specimens (dimensions and numbers *n* in the method sections below) were prepared for

measurement in pristine condition as well as after extraction treatment or control treatment (vapor).

The extraction treatment was conducted at 20 ± 0.5 °C by placing the setup and used solvent in a climate chamber. The setup consisted of a closed glass container filled with solvent to submerge the specimens. As a solvent, deionized water (Milli-Q®) was used with a volume ratio of 1:100. The solvent water was exchanged daily during the 7-d extraction period.

The vapor treatment was equally conducted at 20 ± 0.5 °C by storage in a sealed glass container containing a basin of deionized water for 7 d. Quick saturation of the gas phase was facilitated with an air pump, circulating air bubbles through the water basin. An equivalent saturation in the range of 95% ≤ RH ≤ 100% is achieved with this treatment.

Both treated specimens—after water extraction and vapor treatment—were (re-)conditioned to 20 °C/65% RH after prior conditioning to 20 °C/50% RH, to avoid desorption hysteresis effects.

Moisture sorption analysis

Thin birch sapwood discs of 11 mm diameter and ~ 0.3 mm thickness were produced with the fiber direction along the disc plane and tangential cut surfaces (earlywood region).

Dynamic vapor sorption (DVS) experiments were conducted from 0 to 90% in steps of ~ 10% RH (Figure SI–1) using a *DVS Elevated Temperature* device (Surface Measurement Systems, Wembley, UK). Dry and water-saturated nitrogen gas was mixed with a total flow rate of 3.3×10^{-3} L/s. Each step was held until a constant mass criterion of 0.001%/min was reached. The step response of mass change was recorded every minute by a high-precision electronic balance with 0.1 µg sensitivity.

The adsorption and desorption sequence on the pristine specimens ($n = 6$) was conducted at 23 °C, 30 °C, 40 °C, and 50 °C. The specimens were then subjected to extraction or vapor treatment ($n = 3$, each). After reconditioning the specimens were remeasured at all four temperatures. Finally, in the case of the extracted specimens the measurement at 23 °C was repeated, to be compared to the initial measurement after extraction.

Finally, the DVS sequence was conducted at 23 °C on 12 mg (dry mass) of hydrophilic extractives powder, isolated from wood shavings of the same boards (detailed isolation procedure can be found in Engelhardt et al. 2023).

The specimen mass data of each step were evaluated by fitting to a double-stretched exponential (DSE) function for regression (Eq. 1), as demonstrated in Sánchez-Ferrer et al. (2023):

$$m(t) = m_0 + \left(m_\infty - m_0\right) \cdot \left[P \cdot \left(1 - e^{-(k_1 t)^{\beta_1}}\right) + (1 - P) \cdot \left(1 - e^{-(k_2 t)^{\beta_2}}\right)\right] \quad (1)$$

where k_1 and k_2 are the kinetic constants and β_1, and β_2 the stretching exponents of the exponential decay terms 1 and 2, weighted by $0 < P < 1$. The initial mass at step time $t = 0$ is m_0. The estimated equilibrium mass m_∞ and the dry mass m_{dry} were

used to calculate the equilibrium moisture content $EMC = (m_\infty / m_{dry}) - 1$ of each step.

The EMC step data were then used to generate the corresponding isotherm curves using a modified GAB model by Viollaz and Rovedo (1999), shown (Eq. 2) as a function of water activity (a_w = RH/100%).

$$EMC(a_w) = \frac{M_0 C K a_w}{(1 - K a_w)(1 + (C-1) K a_w)} + \frac{M_0 C K N a_w^2}{(1 - K a_w)(1 - a_w)} \tag{2}$$

Based on this curve, the monolayer water sorption capacity M^0_{SSO} based on Willems' (2014, 2015) sorption site occupancy (SSO) model was estimated, applying the fitting procedure in Sánchez-Ferrer et al. (2023). The concentration of available sorption sites c_{SS} then can be calculated from the estimated monolayer capacity (Eq. 3):

$$c_{SS} = M^0_{SSO} / m w_{H_2O} \tag{3}$$

The equivalent kinetic constant k_{eq} for the DSE function was calculated numerically by solving the function to $m\left(t = {k_{eq}}^{-1}\right) = m_\infty + (m_\infty - m_0) \cdot (1 - e^{-1})$. Based on the assumption of unidirectional diffusion model (Eq. 4) with the geometrical factor (Neogi 1996) of $G = 0.25 \cdot V^2 \cdot A^{-2}$, the apparent diffusion coefficient D_{app}, with the driving potential of moisture concentration C (in kg/m^3), was estimated for the thin disc specimens of volume V and total exposed area A for each sorption step:

$$D_{\text{app}}(RH) = \pi \cdot G \cdot k_{\text{eq}}(RH) \tag{4}$$

The activation energy of diffusion E_a was determined for adsorption steps (Eq. 5) based on the temperature dependence of the diffusivity $D_{\text{app}}(T)$, which exhibits an Arrhenius-like behavior:

$$D_{\text{app}}(T) = D_0 \cdot e^{-\frac{E_a}{RT}} \tag{5}$$

Here, D_0 is a pre-exponential factor, R the molar gas constant, and T the absolute temperature.

Finally, the fitted isotherms (modified GAB model) of each sample at varying temperatures (23 °C–40 °C) were used to calculate the net isosteric heat q_{st} in adsorption, which describes the average binding energy of water to the substrate at a specific concentration. To determine q_{st}, the relation derived from the Clausius–Clapeyron equation (Hill 1949; Iglesias and Chirife 1976) was used (Eq. 6), with the universal gas constant R and the correlation of water activity a_w and absolute temperature T at constant EMC, which was determined by serial linear regressions.

$$q_{st}(\text{EMC}) = -R \cdot \frac{\partial \ln a_w}{\partial T^{-1}} \tag{6}$$

An integration of q_{st} over EMC gives the total binding energy capacity per wood mass Q_{st}, while the asymptotical value toward EMC = 0% (W/W) gives the isosteric heat of the dry substrate $q_{st,0}$, without any water–water interaction.

Swelling and swelling pressure determination

Cubic specimens of $10 \times 10 \times 10$ mm^3 birch sapwood (n = 16) were prepared with side faces cut along the principal directions of the wood. The specimens with a density distribution of 618 ± 23 kg/m^3 (average ± standard deviation) were separated into three groups subjected to (i) no treatment (pristine), (ii) vapor treatment, and (iii) water extraction treatment. By water extraction, an average of 0.64% (W/W) of extractives was removed, corresponding to a degree of extraction of ~ 50% compared to the extractive content results of wood flour samples.

After initial conditioning at 0% RH at 20 °C, each cube was fixed between two parallel polished metal surfaces—a stainless steel bottom plate and a flat aluminum adapter top plate connected to a 500-N load transducer (accuracy < 0.02% F.S.)—at an initial contact force of ~ 1–2 N. The RH was increased in ~ 10% RH steps, held for 24 h each, until reaching ~ 90% RH, and the evolving increases in compressive stress were recorded. For both restricted swelling in the radial and tangential direction, measurements on 12 specimens in a pristine state and after each treatment condition were performed.

In addition to conducting the swelling pressure experiments, the linear swelling coefficients of all specimens and tangential and radial wood direction were determined by comparing the cube dimensions in the dry state (equilibration in silica gel at room temperature) and at the fiber saturation point (FSP). The specimens were conditioned to reach the FSP by repeatedly dipping them in water and storing them in closed containers (~ 95% < RH < 100%) until dimensions stabilized.

Microstructural analysis

The X-ray diffraction (XRD) measurements were taken to observe changes in the amorphous content, *i.e.*, lignin, hemicelluloses, and some cellulose amorphous domains, and in the crystalline cellulose of pristine birch wood specimens and specimens exposed to water extraction. Again, as a control experiment, specimens subjected to vapor treatment were included to differentiate water-based effects from effects of extractives concentration. Before measuring, the specimens were conditioned to 20 °C, 50% RH, and then to 20 °C, 65% RH.

Scattering patterns from XRD on radial cut wood slices ($24 \times 24 \times 1$ mm^3) were determined using a *D8 Advance Eco* diffractometer (Bruker AXS GmbH, Karlsruhe, DE) equipped with a 1-kW $\lambda_{\mathrm{Cu}K\alpha}$ X-ray source. The incident beam was collimated with an automatic divergence slit to 15-mm irradiated sample length and a 2.5° primary soller. The scattering intensity was detected in a scattering angle 2 θ of 2°–40° with 100 steps per degree by a Lynxeye XE-T detector positioned behind a motorized anti-air scatter screen and a 2.5° secondary soller. The exposure time

was set to 0.2 s and increased to 1.0 s in the range $2\theta > 30°$ to improve the signal-to-noise ratio. With this experiment, a scattering wave vector ($4\pi \cdot \sin\theta/\lambda_{Cu,K\alpha}$) of $1.4\ \mathrm{nm}^{-1} < q < 27.9\ \mathrm{nm}^{-1}$ was covered. Thus, the main lattice planes for the crystalline cellulose domains can be calculated by deconvoluting the signal and obtaining the diffraction peaks q_{110}, $q_{1\bar{1}0}$, q_{020} and q_{004}. In Figure SI–2 a graphical representation of the cellulose crystalline unit cell (left) and the cellulose crystallites within the elementary (nano-)fibrils (right) is shown.

Pseudo-Voigt functions (Eq. 5) were fitted to the diffraction pattern via a Levenberg–Marquardt algorithm using *Fityk* (v.1.3.2, GNU GPL 2.0) for peak deconvolution.

$$y(q) = A \cdot \left[\frac{(1-s) \cdot \sqrt{ln(2)}}{\omega \cdot \sqrt{\pi}} \cdot e^{\left[-ln(2) \cdot \left(\frac{q-q_c}{\omega} \right)^2 \right]} + \frac{s}{\pi \cdot \omega \cdot \left[1 + \left(\frac{q-q_c}{\omega} \right)^2 \right]} \right] \tag{7}$$

The unit cell parameters of a monoclinic lattice—the spacings a, b, c, and angle γ—were calculated using Eqs. (8)–(11), following the procedure in Zabler et al. (2010).

$$a = \frac{4\pi}{\sin\gamma \cdot q_{020}} \tag{8}$$

$$b = \sqrt{\left(\frac{\left(q_{1\bar{1}0} + q_{110} \right) \cdot \sin\gamma}{4\pi} \right)^2 - a^{-2}} \tag{9}$$

$$c = \frac{8\pi}{q_{004}} \tag{10}$$

$$\gamma \approx \coth^{-1}\left(\frac{\left(q_{1\bar{1}0} - q_{110} \right) \cdot \sqrt{a^2 + b^2}}{-4\pi} \right) \tag{11}$$

The characteristic correlation lengths ξ_{004} and ξ_{020} corresponding to the length and width of the cellulose microfibrils, respectively, could be estimated from the respective wave vector peak's full-width-at-half-maximum ω using the equation $\xi = 2\pi/\omega$ (Arcari et al. 2019; Bertsch et al. 2019).

Surface property analysis

Contact angle measurements via the sessile drop technique were taken on a *Krüss Easy Drop* with drop shape analysis software *Krüss DSA4*. Alternatively, to using test liquids, which pose various difficulties to use for surface energy evaluations on

porous substrates, wood adhesives were applied directly for simple comparative reasons. A melamine-urea–formaldehyde (MUF) adhesive BASF Kauramin 683/688 (Türmerleim GmbH 2008) (mixing ratio resin/hardener: 100/50 (W/W)) and a one-component polyurethane (PUR) adhesive Loctite HB S709 PURBOND (Henkel and Cie. AG 2015) were applied (15 µL per drop with 18 gauge needles) on newly prepared knife-cut radial surfaces of pristine and extracted wood. In the case of MUF, a new syringe was prepared every 5 measurements to limit viscosity increases due to curing. The contact angles were evaluated using a simple dynamic wetting model (Eq. 12) by Shi and Gardener (2001), to estimate initial and final contact angles θ_i and θ_e, as well as a kinetic factor K, which is a combined measure for the speed of adhesive spreading and penetration.

$$\theta(t) = \frac{\theta_i \cdot \theta_e}{\theta_i + \left(\theta_e - \theta_i\right) \cdot e^{K\left(\frac{\theta_e}{\theta_e - \theta_i}\right)t}} \tag{12}$$

Inverse gas chromatography (IGC) was performed at 25 °C in Henry's law region (infinite dilution method) on both untreated and extracted wood shavings (1–2 g of fraction with mesh size > 300 µm) using a *neuronIC* (Adscientis, Wittelsheim, FR) with a 4-mm column, measuring the retention volume V_G on a series of probe gases. A series of linear alkanes C6–C9 was used to determine the dispersive part of the surface energy γ_s^d (Eq. 13) using the regression procedure by Dorris and Gray (1980).

$$\gamma_s^d = \gamma_{\mathrm{CH_2}}^{-1} \cdot \left(\frac{-R \cdot T \cdot \Delta \ln\left(V_G\right)}{2 \cdot N \cdot a_{\mathrm{CH_2}}} \right)^2 \tag{13}$$

There, $\gamma_{\mathrm{CH_2}}$ is the surface energy of a CH_2 surface (polyethylene) and $a_{\mathrm{CH_2}}$ is the area covered by the adsorption per CH_2 motif (6 $\mathrm{\AA}^2$). Isooctane (2,2,4-trimethylpentane) and cyclooctane were used to estimate the nano-roughness and solubility of the wood surfaces as described by Brendlé and Papirer (1997). Specific (polar) interactions (I_{SP}) were determined with a series of probe gases of known acceptor and donor numbers (Gutmann 1978) to quantify acidic and basic surface interactions.

As the curing of reactive adhesives is affected by acidic or basic compounds in the adherend, the surface pH value of pristine and extracted birch wood was compared to investigate the acidity of the wetted wooden surface. Blocks of 50 × 30 × 10 mm^3 with horizontal annual rings were produced. A drop of 100 µL deionized water was placed on the slice surface with a pipette, and the pH was measured using a QpH 70 m with a Mettler Toledo *Inlab* surface probe. The measurements were taken on aged surfaces (exposed 20 to 30 days in 20 °C/65% RH) and fresh-cut surfaces. Results were evaluated based on the estimated equilibrium by a simple exponential fitting of the development of pH measurement values over 10 min.

Mechanical analysis

The effects of water extraction treatment on mechanical behavior were investigated by measurements of modulus of elasticity E in quasi-static compression experiments. Prismatic specimens of birch wood were cut along the three principal/anatomical directions of wood with the dimensions of 45 (L) × 15 (W) × 15 (T) mm^3. All specimens ($n = 10$ per principal direction) were measured subsequently in pristine condition, after vapor treatment and finally after water extraction treatment.

For strain measurement, a speckle pattern (15×10 mm^2) was applied to the middle of one-side face of the specimens. The deformation of the surface in this region was tracked using a 3D digital-image-correlation system (*Aramis 12 MP variable base*, Carl Zeiss GOM Metrology GmbH, Braunschweig, Germany), giving the average strain in the loading direction (L). Specimen geometry and strain measurement are based on the works of Ożyhar et al. (2013).

The compression experiment was conducted with a universal testing machine (ZwickRoell GmbH & Co.KG, Ulm, Germany) with a 20-kN force transducer (ISO 7500–1 accuracy class 1). The measurement was restricted to the linear visco-elastic regime of the specimens to allow non-destructive, repeatable measurement. Specimens oriented in the longitudinal direction were loaded until 2 kN, and specimens oriented in radial and tangential direction until 0.5 kN and 0.3 kN, respectively. The loading rate was set constant to reach the load limit within 60 s. The evaluation of E was performed via linear regression of the stress–strain data in the interval from 50% to 100% of the respective maximum load.

Results and discussion

Moisture interaction

When using common wood adhesives for structural bonding, the curing process is affected by the adherend's ability to adsorb moisture from the (water-based) adhesive or to provide water to the (*e.g.*, isocyanate-based) adhesive. Therefore, changes in the moisture-sorption behavior of wood will affect the curing dynamics, which can lead to altered bond line formation and adhesion properties. Thus, the moisture interactions of birch wood were studied using dynamic vapor sorption experiments.

The averaged isotherms at 23 °C of 3 specimens, measured in the 23 °C–50 °C temperature range, both in pristine condition (green in Fig. 1A) and after extraction treatment (black curve in Fig. 1A), were analyzed. The extracted specimens' isotherm after a repeated measurement at 23 °C was compared (blue curve in Fig. 1A). A theoretical isotherm was calculated based on mass fractions of extracted wood and extractives, resulting in the hypothetical behavior of a non-interactive mixture of the pristine wood specimens' components (violet dashed line in Fig. 1A). The extractive mass fraction was calculated by the dry mass weight loss by extraction.

The equilibrium moisture content EMC^* was calculated per dry mass of the extracted wood for both the measurements in pristine and extracted specimen conditions. By using the extracted wood mass as a reference for the isotherms, the mass

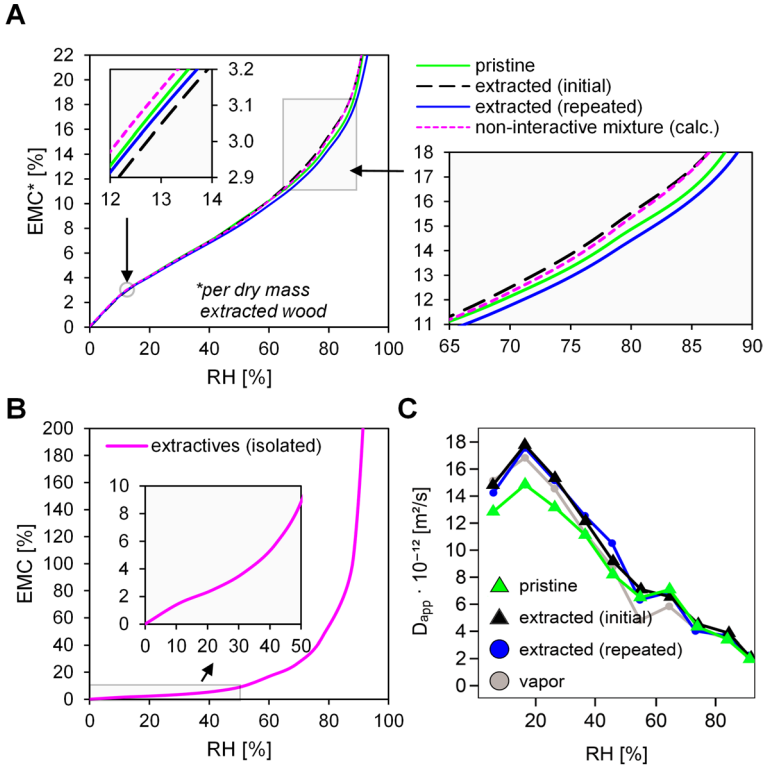

Fig. 1 **A** Moisture adsorption isotherms (axis cutoff at 22%) of birch wood–pristine and after extraction; EMC per dry mass of extracted wood as a function of RH. **B** Moisture adsorption isotherm of the isolated birch extractives sample. **C** Apparent diffusion coefficient D_{app} during the adsorption process for birch wood–pristine, after extraction and vapor treatment

loss due to extraction does not offset the calculated moisture content in the treated specimens. While all wood isotherms showed typical S-shaped curves, the extractives sample's isotherm (Fig. 1B) is dominantly convex in the entire RH range, suggesting it is a Type III isotherm (Sing et al. 1985).

An initial increase in moisture uptake resulted from the extraction treatment when first measured (Fig. 1A, black curve). This difference appeared predominantly in the 70–90% RH (Fig. 1A, right graph) region but not at monolayer sorption levels below 40% RH, as seen in extracted poplar wood by Zhou et al. (2016). A similar multilayer adsorption increase was observed, e.g., by Popper et al. (2006), suggesting a physical bulking action of some pore spaces rather than from hydrogen bonding of extractives to binding sites of wood.

However, the effect of blocked binding sites from hydrogen bonds with extractives in the pristine state on monolayer water concentration could be offset by the additional binding sites of the extractives themselves. Multilayer adsorption might primarily be elevated due to structural changes, *e.g.*, increased nanoporosity or a

local decrease in cellulose crystallinity initially after extraction. This is supported by control experiments with vapor treatment, which observed a similar increase in multilayer absorption, without removing extractives (Figure SI–3). However, a repetition of the isotherm cycle on the extracted specimens showed that the elevated hygroscopicity was only temporary and EMC* during repetition was partly lower than in the pristine state, as seen by Hernández (2007) in the case of the highly hygroscopic acetone extracts from the wood of mahogany and the genus *Copaifera spp*.

The calculated curve of a non-interactive mixture (assuming simple additive behavior of sorption action, purple dashed line in Fig. 1A) of extracted wood (repeated measurement) and extractives does not follow the isotherm of pristine wood but exhibits higher sorption values with an estimated increase twice as high as measured between extracted wood and pristine wood. This is explainable by the affinity of extractives to wood OH groups and clustering of extractives. An alternative version of Fig. 1 can be found in the supporting information in Figure SI–4, where EMC is shown per individual sample dry mass, not dry mass in extracted condition.

Evaluations of sorption site density using the SSO model showed an average sorption site concentration c_{SS} of 7.23 mmol/g in pristine condition. A mostly identical result of 7.24 mmol/g was obtained from the initial measurements after extraction. However, from repeated measurements, 7.07 mmol/g was found on average, corresponding to a 2% decrease in accessible sorption sites after extraction. The isotherms from repeated measurements as well as c_{SS} results are in accordance with the assumption that the moisture uptake capacity reduces when removing a highly hygroscopic fraction. The results also reinforce the hypothesis that the initial increase of moisture content and higher then expected c_{SS} values were due to temporary changes in the wood amorphous polymer conformation caused by water imbibition. The final reduction of c_{SS} indicates a reasonable loss in hydroxyl group concentration by extraction.

Apart from the sorption capacity of the substrate, the kinetics of moisture transport through the adherend's structure can be relevant to the curing behavior of bond lines. Hygroscopic substances present in the extractives can affect the retention of water vapor while diffusing through the wood. Therefore, the dynamic vapor sorption experiments were analyzed to estimate the apparent water diffusivity of the untreated and extracted birch wood specimens. The apparent diffusivity D_{app} reduces strongly with higher RH due to changing cell wall rheology but also increasing latent heat effects (Willems 2020). In adsorption, at 23 °C (Fig. 1C), the highest diffusivity was calculated at the step from 10 to 20% RH with $15{\cdot}10^{-12}$ m^2/s for pristine wood and $18{\cdot}10^{-12}$ m^2/s for extracted wood. At 50% RH, values of D_{app} converge to similar values of $6{\cdot}10^{-12}$ µm^2/s, further reducing at higher RH levels. Therefore, only minor changes in diffusion kinetics were observed after extraction. Besides, the evaluations showed no significant differences to pristine state specimens at higher temperatures as well as the comparative measurements of vapor-treated specimens. The calculated diffusivity D_{app} profiles for all measured temperatures are shown in adsorption and desorption steps in Figure SI–5.

The activation energy of diffusion E_A was similar for extracted and pristine birch wood, with no significant differences between treatment groups. At low relative humidity levels (evaluated from 0 to 10% RH adsorption step), E_A was highest with ~ 40 kJ/mol, decreasing toward higher relative humidity and trending toward the value for self-diffusion of water of ~ 18 kJ/mol (Mills 1973; Fripiat et al. 1984), as shown in Figure SI–7. These results are in good accordance with the estimations of Skaar (1988) for E_A of 40.2 kJ/mol in dry state, based on data of longitudinal cell wall diffusion experiments (Stamm 1959) of Sitka spruce, suggesting little inter-specific variation. Other studies, however, found clear differences between wood species, *e.g.*, between poplar and oak (Kang and Hart 1997). As E_A calculation approaches differ (Hunter 1992) and are derived from diffusivity values, the calculation of which is also manifold (Higuchi 1961; Choong and Skaar 1972; Ritger and Peppas 1987; Peleg 1988; Wadsö 1994; Avramidis et al. 1994; Olek and Weres 2007; Thybring et al. 2019), comparing these study results with existing data in more detail would be challenging.

The net isosteric heat was evaluated using the isotherm data of sorption experiments at 23 °C (repetition measurement), 30 °C, and 40 °C. In dry conditions, for pristine and extracted specimens, the sorption enthalpy $q_{st,0}$ (Figure SI–8A) was on average 8.1 kJ/mol and 6.9 kJ/mol (− 15%), and the average total isosteric heat of wetting Q_{st} (Figure SI–8B) was 24 J/g and 17 J/g (− 29%), respectively. Therefore, the evaluations suggest that pristine specimens exhibit stronger hydrogen bonds between water and the extractives fraction compared to the wooden biopolymer substrate, which can result from the higher mobility of extractives, allowing better alignment of the directional hydrogen bonds (q_{st} under optimal conditions, i.e., in vapor phase for O–H···O bonds can reach 21 kJ/mol (David et al. 2017)). While variation of $q_{st,0}$ results was high, with largely overlapping distributions for the pristine and extracted treatment groups, Q_{st} was significantly lowered ($p < 0.003$) in the case of extracted specimens. The obtained results are generally in good agreement with literature data on multiple coniferous woods (Koumoutsakos and Avramidis 1999), suggesting limited inter-specific variation. Significantly lower results were obtained for tropical wood species by Simo-Tagne et al. (2019), which can, however, also be a result of the isotherm model (Nelson Jr 1983) applied there. As sorption enthalpy falls to near-zero levels at moisture contents above equilibrium moisture contents of 9%(W/W) (Figure SI–8C), the additional isosteric heat in practical gluing applications is negligibly small.

In summary, the observed changes in sorptive capacity are small in terms of their practical relevance regarding the glueability of the wood. The effect size is well within the typical intra-specific variances of vapor sorption, which are to be expected in industrial wood assortments.

Swelling behavior

In environments of varying humidity, wood adhesive bonds are subject to additional stresses due to the swelling and shrinking of wood and the resulting stresses due to the restricting action of the adhesive. Both removing a hygroscopic extractives

fraction from the cell walls and effects from water imbibition itself were suspected to potentially change the swelling properties of birch wood. Therefore, the swelling pressure exerted on cubic specimens, restricted in the radial and tangential directions upon stepwise relative humidity increase, was measured and analyzed. Additionally, the dimensional increase at the fiber saturation point due to free swelling, compared to the dimension in the dry state, was determined.

At levels above 90% RH, significant yielding and plasticization behavior showed, so the swelling pressure experiments were evaluated in the < 85% RH range. There, the swelling pressures reached within the 24-h periods correlated fairly linearly with RH ($R2 > 0.97$ for all specimens). The equilibrium swelling pressure as a function of RH is shown for the control group (pristine) and the treatment groups (vapor and extraction) in Fig. 2A and B for restriction in radial and tangential direction, respectively. The distributions of the linear swelling pressure coefficient LSPC, as the gradient of swelling pressure as a function of water activity a_w, estimated by linear regression, are summarized in Fig. 2C.

In the case of specimens restricted in the radial direction, the average LSPC of specimens in pristine condition was 1.7 MPa. For specimens subjected to vapor or extraction treatment, LSPC was reduced to 1.5 MPa. When restricted in the tangential direction, the average LSPC of specimens in pristine condition was 1.9 MPa and reduced to 1.6 MPa and 1.5 MPa after vapor and extraction treatment, respectively. Since both treatments reduced swelling pressure, it can be attributed only to a fractional extent to the removal of extractives. The imbibition of water and its well-known plasticization effect seems to allow for a reorganization of the glassy polymers within the cell walls, leading to the observed effects. However, added free volumes due to extractives removal can additionally lower swelling pressure. In the supplementary information, swelling pressure p_s and density-specific swelling pressure p_s/ρ as functions of RH and EMC are shown (Figure SI–9). When extrapolating the pressure data of pristine birch wood (linear regressions in Fig. 2) to 100% RH, average tangential and radial pressures of 1.9 MPa and 1.8 MPa are obtained. The observed pressures in the tangential direction achieved similar levels as found for pine sapwood with 1.3 MPa (Rybarczyk and Ganowicz 1974). Swelling pressure

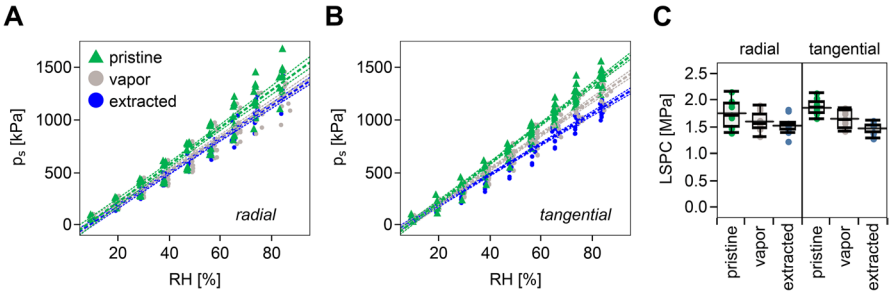

Fig. 2 Equilibrium swelling pressure p_s as a function of RH for steps in the range of 10–90% RH for uniaxial restriction in **A** radial and **B** tangential direction, separated by treatment type. The dashed lines indicate linear regression results and the confidence bands ($\alpha = 0.05$). **C** The distributions of linear swelling pressure coefficients (LSPC) are shown in boxplots for each direction and treatment type

from dry to submerged state was found to have a more distinct anisotropy in the case of pine softwood with 1.6 MPa and 1.0 MPa when specimens were restricted in tangential or radial direction, respectively (Raczkowski 1962, 1970). For hardwoods, high tangential swelling pressures of 3–4 MPa—and even higher values—were measured (Perkitny et al. 1959; Perkitny and Helinska 1963). Immersion experiments are difficult for comparison since strong stress relaxation phases after reaching a swelling pressure maximum can occur, as seen also for birch wood by Keylwerth (1962). Moreover, comparisons between studies of swelling pressure can be impractical due to methodological differences like specimen geometry, which was rather small in this study, allowing high degrees of lateral expansion. This can explain lower results of swelling pressure in unidirectional restricted setups. Other factors affecting measurement results are, *e.g.*, specimen shape, applied initial pressure, force measurements and compensation of transducer strain, and parameters like temperature.

The dimensional change from dry condition to fiber saturation point was compared in both radial and tangential directions. In the tangential direction, the average dimensional increase was 11.4% for pristine wood specimens. The tangential swelling after vapor and extraction treatment was 11.1% and 11.6% on average, respectively. Therefore, the tangential swelling behavior was mostly unaffected by both treatments. In the radial direction, however, the average expansion was 5.3% for pristine wood specimens but increased to 5.9% after vapor treatment and 6.7% after extraction treatment, which constitutes a relative increase of 25%. Individual results are shown as boxplots in Figure SI–10. No verification data from the literature were available regarding the effects of extractives. Regarding the maximum swelling for silver birch in general, Schwab (2000) cited higher results of 12.4% and 7.1% for maximum tangential and radial swelling of birch wood, respectively, while Giebeler (1983) determined somewhat lower tangential swelling of 9% and in the radial direction of 6%, corresponding to a swelling ratio (tangential/radial) of 1.5. While other authors found this ratio was higher as 1.9 (Kumar 1957) or lower as 1.4 (Noack et al. 1973), in this study, it was 2.2 in pristine condition but reduced to 1.9 and 1.7 after vapor and extraction treatment, respectively.

Microstructural characteristics

The observed variations of sorption and swelling behavior, also occurring after vapor treatment without extraction, were suspected to be connected to modifications of the biopolymer conformation. To test this hypothesis, pristine and treated specimens of birch wood were characterized via X-ray diffraction for a comparative analysis.

After applying a baseline correction and the pseudo-Voigt peak deconvolution on the corrected diffraction patterns, the following peaks associated with amorphous and crystalline domains and the respective peak parameters were evaluated. For pristine birch wood specimens, the two peaks related to amorphous domains (large peak area and ω-to-height ratio > 20) centered at the scattering vector values $q_{A1} = 13.9\ \mathrm{nm}^{-1}$ and $q_{A2} = 24.5\ \mathrm{nm}^{-1}$ (red peaks in Fig. 3A), while in the case of peaks

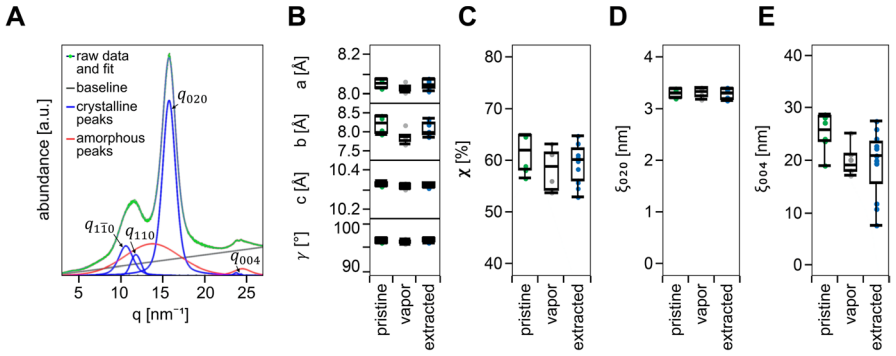

Fig. 3 Evaluation results of X-ray diffraction measurements. **A** exemplary XRD pattern (intensity as a function of the scattering vector q) and peak deconvolution for pristine silver birch wood. Distributions by treatment type of **B** lattice parameters a, b, c, and γ; **C** degree of crystallinity χ; **D** correlation length ξ_{020} along b-axis (nanofibril width estimate); **E** correlation length ξ_{004} along c-axis (cristallite length)

associated with cellulose crystallites (blue peaks in Fig. 3A) at $q_{110} = 11.6\ \text{nm}^{-1}$, $q_{1\bar{1}0} = 10.4\ \text{nm}^{-1}$, $q_{020} = 15.7\ \text{nm}^{-1}$ and $q_{004} = 24.3\ \text{nm}^{-1}$, on average. The average full-width-at-half-maximum ω_{020} and ω_{004} were 1.91 nm^{-1} and 0.25 nm^{-1} for pristine wood, respectively. The calculated monoclinic lattice parameters from the peak fittings (Fig. 3A) for pristine birch wood were $a = 8.1$ Å, $b = 8.2$ Å, $c = 10.3$ Å, and $\gamma = 96.4°$. These values are in reasonable accordance with measurements of crystalline cellulose domains in recent literature (Bertsch et al. 2019; Lee et al. 2019; Penttilä et al. 2020; Viljanen et al. 2020) and were very similar for the treated wood specimens. The degree of crystallinity χ, as the fraction of crystalline peak areas to the total signal area after baseline correction, was subject to high variance (±3% standard deviation within groups). The absolute values of χ are also affected by the method of baseline correction and, therefore, higher than expected (Fengel and Wegener 1983; Andersson et al. 2003) and considered preferably for contrasting juxtaposition of treatments only. The distributions (Fig. 3B) indicate a minor reduction in crystallinity from an average of 61% in pristine conditions to 58% after vapor and 59% after extraction treatment, corresponding to a 3–5% lower crystallinity in relative terms.

Peak width comparisons revealed stable average widths of the nanofibrils with $\overline{\xi_{020}}$ of 3.1 nm–3.2 nm (Fig. 3C) for all specimen groups. However, the nanofibril length evaluation (Fig. 3D) gave an average value of $\overline{\xi_{004}}$ of 25.2 nm for specimens in pristine condition but lower values of 19.9 nm and 19.5 nm after vapor treatment and extraction treatment, respectively, indicating that water converts the edges along the fiber direction of the crystalline domains into amorphous cellulose or increases the disorder in the transition phase between crystalline and amorphous domains. The change of correlation length corresponds to a reduction of the average characteristic number of glucose units in cellulose crystallites $\Delta n_{glucose} = \Delta\overline{\xi_{004}} \cdot 2/c$ of 10–11, *i.e.*, a reduction from 49 in pristine condition to 39 and 38 after vapor and extraction treatment, respectively. The evaluation suggests that both the vapor treatment and the extraction treatment with water led to a measurable increase in the disorder of

cellulose microfibrils. The peak parameters from fitting and the lattice parameters are summarized in Table SI–1 and Table SI–2.

Bonham and Barnett (2001) performed X-ray diffraction measurements on birch wood to measure microfibril angle (MFA) using Evans' (1999) method, which is not possible with the data in this study due to the azimuthal integration during measurement. In Peura et al. (2008), lattice parameters of cellulose in birch wood were also determined; however, only changes due to mechanical stresses were published, with no absolute values. There, in dry condition, a lower microfibril width ξ_{020} of 2.8 nm and length ξ_{004} of 20 nm were found. In Leppänen et al. (2011), ξ_{020} of 3.2 nm and 2.9 nm was found for green and air-dried birch wood, respectively. Generally, a reasonable agreement with the available literature data on silver birch wood was obtained.

Surface properties

Since the wetting behavior is a glueability-related quality of the adherend and changing the chemical composition by extraction can result in its modification, a series of measurements were conducted to evaluate the surface properties of birch wood in the context of extractives presence. As opposed to determining surface energy characteristics by contact angles with test liquids, a direct approach using MUF and PUR wood adhesives for contact angle measurements was conducted on pristine and extracted wood specimens to evaluate how wetting with the liquid adhesives is affected. Due to the adhesive's viscous nature, the contact angle's development was observed over time and analyzed with a simple model (Eq. 12) by Shi and Gardner (2001). The final contact angle of sessile MUF adhesive drops was $57° \pm 6°$ (average $\pm$ standard deviation) on untreated birch wood substrate. On extracted wood, the final contact angle was slightly higher with a value of $62° \pm 4°$. In the case of PUR adhesive drops, the final contact angle was $60° \pm 3°$ and $63° \pm 2°$ on pristine wood substrate surfaces and extracted surfaces, respectively. Interestingly, the change after extraction was very similar in the cases of both the hydrophilic, water-based MUF and the hydrophobic PUR drops. However, given the variance of the results within measurement groups, the raises of average contact angles by 4° (MUF) and 3° (PUR) after extraction are small. More detailed contact angle measurement results and evaluation results can be found in the supplementary information (Table SI–3 and Figure SI–11).

Since wetting is considered an integral part of the wood bonding process, the affinity of solids to be wetted by liquids is further analyzed by determination of the surface energy properties using inverse gas chromatography (IGC). Only minor differences in surface energy characteristics between samples were observed. The calculated dispersive surface energy γ_s^d of the pristine and extracted birch sample was 39.3 ± 0.2 and 38.4 ± 0.2 mJ/m^2, respectively. The absolute values of γ_s^d should be interpreted cautiously, as probing with isooctane and cyclooctane revealed both soft domains and solubility effects with these samples. The extracted wood sample was more extreme in this regard, showing higher solubility effects and stronger size exclusion effects. This was quantified based on the morphological

indices $IM_{cyclooctane}$ and RIM, which were 1.4 and 2.2 for the pristine wood, while for extracted wood were 1.5 and 2.7, respectively. The extracted wood also showed slightly more polar characteristics with a sum of specific interactions $\sum I_{SP}$ of 84.2 kJ/mol *vs*. 82.6 kJ/mol for pristine wood. Detailed results are found in the supporting information (Table SI–4 and Figure SI–12). The determined γ_s^d was slightly lower than older data of white birch by Kamdem et al. (1993) with similar I_{SP} results. As opposed to spruce and pine softwoods, where extraction led to significantly higher γ_s^d (Tshabalala 1997; Liu et al. 1998; Walinder and Gardner 2000) because of the nonpolar nature of the removed resins, the hydrophilic birch extractives are of more similar polarity and present in small quantities, thus not affecting surface energy significantly. Increased $\sum I_{SP}$ and a slightly higher γ_s^d of 39 mJ/m^2 vs. 37 mJ/m^2 after hot-water extraction was found by Oporto et al. (2011), although based on measurements on an undefined hardwood mixture. In summary, similar morphology, dispersive surface energy, and specific interaction characteristics were observed for both specimens. The variations are not expected to affect the glueability of the wood in terms of wettability with the adhesives to a degree of any practical relevance.

For most reaction adhesives, the acidity during curing affects the reaction rate or even the occurring reaction types. To observe the change in acidity of the wooden substrate due to extraction, pH measurements on freshly cut surfaces showed an increase from 5.4 on average in pristine conditions to 6.3 after extraction treatment. This corresponds to a decline of H^+ concentration by 87%. After an aging period of 20–30 d, the average pH of pristine and extracted wood surfaces was slightly reduced to 5.1 and 6.1, respectively. This aging effect was, therefore, independent of extractive concentration. The results are also shown as boxplots in the supplementary information (Figure SI–13). These results show the acidic nature of the hydrophilic extractives in birch wood and, therefore, the neutralizing effect of the extraction procedure. The acidity can affect the curing behavior of reactive adhesives such as phenol–formaldehyde formulations or MUF adhesives (Engelhardt et al. 2023) by accelerating or retarding the reaction.

Mechanical properties

The observed effects of water imbibition, especially the increased amorphous scattering and reduced correlation lengths of microfibril crystallite regions via X-ray diffraction measurements, justify an assumption of changes in mechanical properties. To check and quantify this, the effects of water treatments on mechanical properties were investigated by determination of the modulus of elasticity E in compression at a constant stress rate in the linear-viscoelastic (LVE) regime. Prismatic specimens in all principal directions (each $n = 10$) were measured subsequently in untreated condition (pristine), after vapor treatment and reconditioning (vapor), and after water extraction treatment and reconditioning (extracted).

E_L in the longitudinal direction (Fig. 4A) showed an average of 19.3 GPa, 18.2 GPa, and 17.2 GPa for pristine, vapor-treated and extracted specimens, respectively. In the radial loading direction (Fig. 4B), the average E_R was 1.24 GPa, 1.16 GPa,

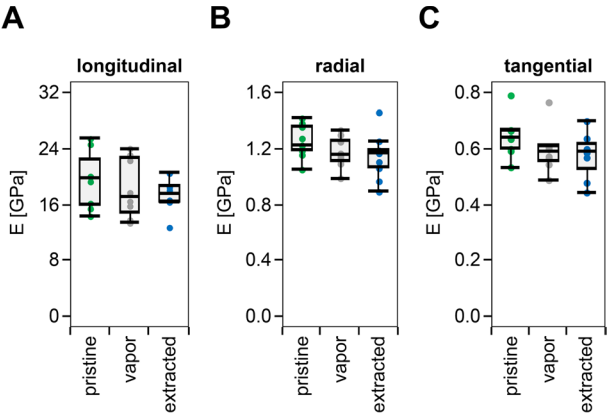

Fig. 4 Distribution of elastic moduli E in compression mode on birch wood specimens loaded in **A** longitudinal, **B** radial, and **C** tangential direction in pristine condition, after vapor treatment, and after water extraction treatment, respectively

and 1.09 GPa, while in tangential loading direction (Fig. 4C) E_T was 0.64 GPa, 0.59 GPa, and 0.57 GPa for pristine, vapor-treated, and extracted specimens, respectively.

Since identical specimens were measured before and after treatment, the resulting data set was statistically analyzed using the paired t test to estimate the significance p of mean differences. In summary, both the vapor treatment and the water extraction treatment resulted in very similar effects on the stiffness of birch wood, with an average decrease of E_L of 10–11% in the fiber direction ($p \leq 0.05$) after both water treatments. In radial and tangential directions, the average reduction of E_R and E_T after extraction treatment was 11–12%, while vapor treatment caused only a ~ 7% reduction ($p \leq 0.05$ for tangential and $p \leq 0.005$ for radial loaded specimens, respectively). The median levels of E, however, show very similar behavior with a decrease of 8% in both of the perpendicular directions. The results of individual measurements are listed in the supplementary information (Table SI–5).

Considering simple comparisons of E for pristine birch wood, a good agreement was observed with the available literature data, e.g., by Hörig (1935), where E_L was given with 16.4 GPa, E_R was 1.11 GPa, and E_T 0.62 GPa. In Grabner et al. (2005), a lower E in transverse compression after extraction of larch wood was associated with the then missing bulking action of extract depositions in the porous structure. The slightly increased effect on E after extraction compared to the vapor-treated wood could stem from added free volume and loss of non-covalent crosslinking via hydrogen bonding of extractives. However, this might also be related to the fact that the extraction likely achieves a higher cell wall saturation than the vapor treatment. Considering the similar results of vapor-treated and extracted specimens, the measurements suggest that the cause of the softening effect seen in this study was—besides the removal of water-extractable compounds—to a large degree due to the high-water adsorption phase.

Conclusion

This study performed a broad screening of selected adhesion-related properties of silver birch wood. A focus was placed on the comparative analysis of the characteristics in untreated (pristine) conditions *vs.* following water extraction treatments. Where appropriate, control experiments following a vapor treatment were conducted to differentiate between extractives-related effects and effects due to the extraction procedure, *i.e.*, the water imbibition.

The extraction treatment of birch wood with water resulted in an initially increased multilayer sorption, which after repeating sorption cycles reversed to a reduction of moisture sorption in the multilayer domain and slightly in the monolayer domain. While the effect on the multilayer is expected to result from the increase in free volume, the monolayer is influenced by a positive net effect of extractives on binding sites by providing more OH groups compared to their occupancy. Therefore, the hydrophilic extraction resulted in a decrease in sorption site concentration c_{ss} of 2.2%. Both factors are also suspected to be attributed to the observed increase in moisture diffusivity at room temperature and low RH. Given their increased mobility, extractives can align better and with higher denticity (number of binding sites for water molecule) and, therefore, establish stronger hydrogen bonding, which was reflected in a calculated loss of isosteric heat $q_{st,0}$ of 15% after extraction.

The free swelling slightly increased while swelling pressure was reduced after extraction. Measurements after vapor treatment indicate the effect is mostly related to the water imbibition, namely a change in polymer configuration and lowered crystallinity, allowed by the plasticization of water, instead of the removal of extractives, which has a minor effect, possibly due to the creation of additional free volume.

The structural investigation via X-ray diffraction analysis showed a 5% decrease in the degree of crystallinity χ, likely related to the reduction of the characteristic length of cellulose crystallites ξ_{004}. These results can also indicate that the wood biopolymers shifted toward a higher disordered state after both water treatments. The changes in the X-ray diffraction patterns, as well as the reduced swelling pressure, are likely connected to the mechanical properties, as a reduction in the average modulus of elasticity E by 10% to 12%, depending on the loading direction, was determined using compression tests.

The wetting behavior was only marginally affected by hydrophilic birch wood extractives. Both contact angle measurements and inverse gas chromatography did not reveal significant differences in surface energy properties due to extraction. Only a lowered acidity was detected with surface pH measurements.

In summary, water as a plasticizer allows a reconfiguration of the glassy polymer backbone of wood and may disorder the ends of crystallites in cellulose nanofibril chains. The removal of extractives might enhance some of the observed effects (mechanical softening, swelling pressure reduction, structural changes), physically due to additional free volume and missing bulking action and chemically due to extractives hydrogen bonding.

In practical terms, the variation of the investigated bulk and surface properties due to the presence of extractives is assessed as small with regard to the implications on usability for bonded wood products. None of the performed comparative studies indicate problematic moisture sorption-related property changes, dimensional stability issues, surface energy deterioration, or considerable changes in mechanical properties due to the presence of hydrophilic extractives in birch wood. In contrast to more problematic wood species, with higher property variations due to extractives, silver birch wood thus offers relatively stable bulk and surface properties in this regard.

Further research could consider the permanence of the observed effects. Wood, in constant interaction with environments of varying humidity, is never in an equilibrium state, and the effects seen due to water or vapor exposure can be assumed to be subject to change over time.

Supplementary Information The online version contains supplementary material available at https://doi.org/10.1007/s00226-023-01526-x.

Acknowledgements We thank Dr. Ralf Dümpelmann (Inolytix AG), Nesrine Debabèche, and Dr. Eric Brendle (Adscientis) for their support with inverse gas chromatography measurements. We also thank the staff of Holzforschung München, especially Frank Moosmann and Roland Braun, for their continuous and unconditional support of our research activities.

Author contributions ME designed the study, performed the experiments on moisture sorption, swelling behavior mechanical behavior. ME further conducted the evaluations and analyses of the experimental data and wrote the manuscript. AG performed the XRD experiments. KR supervised the study and contributed to the discussion of the results and manuscript polishing. ASF designed the study, analyzed data, supervised the experimental work and contributed to the writing of the manuscript.

Funding Open Access funding enabled and organized by Projekt DEAL.

Declarations

Conflict of interest The authors declare no competing interests.

References

Andersons B, Andersone I, Biziks V et al (2009) Hydrothermal modification for upgrading the durability properties of soft deciduous wood. In: The 41 Annual Meeting of IRG-WP. IRG Secretariat, Biarritz, France

Andersson S, Serimaa R, Paakkari T et al (2003) Crystallinity of wood and the size of cellulose crystallites in Norway spruce (Picea abies). J Wood Sci 49:531–537. https://doi.org/10.1007/s10086-003-0518-x

Arcari M, Zuccarella E, Axelrod R et al (2019) Nanostructural properties and twist periodicity of cellulose nanofibrils with variable charge density. Biomacromolecules 20:1288–1296. https://doi.org/10.1021/acs.biomac.8b01706

Ashburner K, McAllister HA, Rix M (2013) The genus Betula: a taxonomic revision of birches. Kew publishing, London

Avramidis S, Hatzikiriakos SG, Siau JF (1994) An irreversible thermodynamics model for unsteady-state nonisothermal moisture diffusion in wood. Wood Sci Technol 28:349–358. https://doi.org/10.1007/BF00195282

Baumann G, Brandner R, Müller U et al (2020) Temperature-related properties of solid birch wood under quasi-static and dynamic bending. Materials 13:5518. https://doi.org/10.3390/ma13235518

Bertsch P, Sánchez-Ferrer A, Bagnani M et al (2019) Ion-induced formation of nanocrystalline cellulose colloidal glasses containing nematic domains. Langmuir 35:4117–4124. https://doi.org/10.1021/acs.langmuir.9b00281

Bonham VA, Barnett JR (2001) Fibre length and microfibril angle in silver birch (betula pendula Roth). Holzforschung 55:159–162. https://doi.org/10.1515/HF.2001.026

Bouffard J-F, Blanchet P, Barbuta C (2010) Long-term performance of engineered wood flooring with oriented strand board substrate. For Prod J 60:508–513. https://doi.org/10.13073/0015-7473-60.6.508

Brendlé E, Papirer E (1997) A new topological index for molecular probes used in inverse gas chromatography for the surface nanorugosity evaluation. J Colloid Interface Sci 194:207–216. https://doi.org/10.1006/jcis.1997.5104

Cakiroglu EO, Demir A, Aydin I (2019) Comparison of birch and beech wood in terms of economic and technological properties for plywood manufacturing. Drv Ind 70:169–174. https://doi.org/10.5552/drvind.2019.1828

Choong ET, Achmadi SS (1991) Effect of extractives on moisture sorption and shrinkage in tropical woods. Wood Fiber Sci 23:185–196

Choong ET, Skaar C (1972) Diffusivity and surface emissivity in wood drying. Wood Fiber Sci 4:80–85

David V, Grinberg N, Moldoveanu SC (2017) Long-range molecular interactions involved in the retention mechanisms of liquid chromatography. In: Grinberg Nelu, Grushka Eli (eds) Advances in Chromatography, 1st edn. CRC Press, Boca Raton

Dorris GM, Gray DG (1980) Adsorption of n-alkanes at zero surface coverage on cellulose paper and wood fibers. J Colloid Interface Sci 77:353–362. https://doi.org/10.1016/0021-9797(80)90304-5

Dubois H, Verkasalo E, Claessens H (2020) Potential of birch (*Betula pendula* Roth and B. pubescens Ehrh.) for forestry and forest-based industry sector within the changing climatic and socio-economic context of Western Europe. Forests 11:336. https://doi.org/10.3390/f11030336

Ehrhart T, Brandner R, Schickhofer G, Frangi A (2015) Rolling shear properties of some European timber species with focus on cross laminated timber (CLT): test configuration and parameter study. Timber Scientific Publishing, Šibenik

Engelhardt M, Böger T, Gigl M et al (2023) Interactions of hydrophilic birch wood (*Betula pendula* Roth) extractives with adhesives for load-bearing timber structures. Int J Adhes Adhes 125C:103447. https://doi.org/10.1016/j.ijadhadh.2023.103447

Evans R (1999) A variance approach to the X-ray diffractometric estimation of microfibril angle in wood. Appita J 52:283–289

Fengel D, Wegener G (eds) (1983) Chemical composition and analysis of wood. In: Wood De Gruyter, pp 26–65

Fleer FG (2019) Birch structural timber - distribution of strength related wood characteristics and their influence on bending properties (Birkenkonstruktionsholz - Verteilung Festigkeitsprägender Holzeigenschaften und deren Einfluss auf das Biegeverhalten). Master's Thesis, Georg-August-Universität Göttingen

Frihart CR (2007) Model for Understanding the durability performance of wood adhesives. In: Proceedings 30th annual meeting of the adhesion society, Inc. Tampa Bay, FL, US, pp 222–224

Fripiat JJ, Letellier M, Levitz P (1984) Interaction of water with clay surfaces. Philos Trans R Soc Lond Ser Math Phys Sci 311:287–299. https://doi.org/10.1098/rsta.1984.0029

Giebeler E (1983) Dimensional stabilization of wood through a moisture/heat/pressure treatment (Dimensionsstabilisierung von Holz durch eine Feuchte/Wärme/Druck-Behandlung). Holz Roh- Werkst 41:87–94. https://doi.org/10.1007/BF02608498
Türmerleim GmbH (2008) Kauramin® resin 683 liquid with Kauramin® hardener 688 liquid in wood construction, technical data sheet (German). Türmerleim GmbH, Ludwigshafen
Grabner M, Müller U, Gierlinger N, Wimmer R (2005) Effects of heartwood extractives on mechanical properties of larch. IAWA J 26:211–220. https://doi.org/10.1163/22941932-90000113
Grinins J, Biziks V, Marais BN et al (2021) Weathering stability and durability of birch plywood modified with different molecular weight phenol-formaldehyde oligomers. Polymers 13:175. https://doi.org/10.3390/polym13020175
Gutmann V (1978) The donor-acceptor approach to molecular interactions. Plenum Press, New York
Henkel & Cie. AG (2015) LOCTITE® HB S309 PURBOND, Technical Data Sheet (German). Henkel & Cie. AG Sempach Station
Hernández RE (2007) Moisture sorption properties of hardwoods as affected by their extraneous substances, wood density, and interlocked grain. Wood Fiber Sci 39:132–145
Higuchi T (1961) Rate of release of medicaments from ointment bases containing drugs in suspension. J Pharm Sci 50:874–875. https://doi.org/10.1002/jps.2600501018
Hill TL (1949) Statistical mechanics of adsorption. V. Thermodynamics and heat of adsorption. J Chem Phys 17:520–535. https://doi.org/10.1063/1.1747314
Hofferber BM, Kolodka E, Brandon R et al (2006) Effects of swelling forces on the durability of wood adhesive bonds. In: Proceedings of the 29th annual meeting of the Adhesion Society, Inc. Jacksonville, FL, US, pp 187–189
Hörig H (1935) Application of the theory of elasticity of anisotropic bodies to measurements on wood (Anwendung der Elastizitätstheorie anisotroper Körper auf Messungen an Holz). Ing-Arch 6:8–14. https://doi.org/10.1007/BF02086407
Hunter AJ (1992) On the activation energy of diffusion of water in wood. Wood Sci Technol. https://doi.org/10.1007/BF00194464
Iglesias HA, Chirife J (1976) Isosteric heats of water vapor sorption on dehydrated foods. I. Analysis of the differential heat curves. Lebensm-Wiss -Technol 9:116–122
Jeitler G, Augustin M (2016) Is birch the better beech? Grading, processing and mechanical properties of birch Glulam and birch CLT (Ist Birke die bessere Buche? Mechanische Eigenschaften und Referenzprojekte aus BIRKE|BSH&BSP). In: Tagungsband Internationales Holzbau-Forum (IHF 2016). Garmisch
Kamdem DP, Bose SK, Luner P (1993) Inverse gas chromatography characterization of birch wood meal. Langmuir 9:3039–3044. https://doi.org/10.1021/la00035a049
Kang H-Y, Hart CA (1997) Temperature effect on diffusion coefficient in drying wood. Wood Fiber Sci 29:325–332
Keylwerth R (1962) Investigations on the free and restraint swelling—Part II: restraint swelling (Untersuchungen über freie und behinderte Quellung—Zweite Mitteilung: Behinderte Quellung). Holz Roh-Werkst 20:292–303. https://doi.org/10.1007/BF02608540
Koumoutsakos A, Avramidis S (1999) Enthalpy-entropy compensation in water sorption by various wood species. Holz Roh-Werkst 57:379–382. https://doi.org/10.1007/s001070050363
Kumar VB (1957) The influence of organic liquids on the mechanical properties of wood (Der Einfluß organischer Flüssigkeiten auf mechanische Eigenschaften des Holzes). Holz Als Roh- Werkst 15:423–432. https://doi.org/10.1007/BF02609533
Lee C-G, Yamasaki M, Sugimoto T, Sasaki Y (2019) Synchrotron X-ray measurements of cellulose in wood cell wall layers of Pinus densiflora in the transmission and reflectance modes. Part 1: results without loading. Holzforschung 73:613–619. https://doi.org/10.1515/hf-2018-0120
Leppänen K, Bjurhager I, Peura M et al (2011) X-ray scattering and microtomography study on the structural changes of never-dried silver birch, European aspen and hybrid aspen during drying. Holzforschung 65:865–873. https://doi.org/10.1515/HF.2011.108
Liu FP, Rials TG, Simonsen J (1998) Relationship of wood surface energy to surface composition. Langmuir 14:536–541. https://doi.org/10.1021/la970573y
Mills R (1973) Self-diffusion in normal and heavy water in the range 1–45.deg. J Phys Chem 77:685–688. https://doi.org/10.1021/j100624a025
Nelson RM Jr (1983) A model for sorption of water vapor by cellulosic materials. Wood Fiber Sci 15:8–22
Neogi P (ed) (1996) Diffusion in polymers. Marcel Dekker, New York

Noack D, Schwab E, Bartz A (1973) Characteristics for a judgment of the sorption and swelling behavior of wood. Wood Sci Technol 7:218–236. https://doi.org/10.1007/BF00355552

Nzokou P, Kamdem P (2004) Influence of wood extractives on moisture sorption and wettability of red oak (*Quercus rubra*), black cherry (*Prunus serotina*), and red pine (*Pinus resinosa*). Wood Fiber Sci 36:483–492

Olek W, Weres J (2007) Effects of the method of identification of the diffusion coefficient on accuracy of modeling bound water transfer in wood. Transp Porous Media 66:135–144. https://doi.org/10.1007/s11242-006-9010-6

Oporto GS, Gardner DJ, Kiziltas A, Neivandt DJ (2011) Understanding the affinity between components of wood-plastic composites from a surface energy perspective. J Adhes Sci Technol 25:1785–1801. https://doi.org/10.1163/016942410X525759

Ozyhar T, Hering S, Niemz P (2013) Moisture-dependent orthotropic tension-compression asymmetry of wood. Holzforschung 67:395–404. https://doi.org/10.1515/hf-2012-0089

Peleg M (1988) An empirical model for the description of moisture sorption curves. J Food Sci 53:1216–1217. https://doi.org/10.1111/j.1365-2621.1988.tb13565.x

Penttilä PA, Altgen M, Carl N et al (2020) Moisture-related changes in the nanostructure of woods studied with X-ray and neutron scattering. Cellulose 27:71–87. https://doi.org/10.1007/s10570-019-02781-7

Perkitny T, Helinska L (1963) Swelling pressure of wood in water and water-saturated air (Der Quellungsdruck des Holzes in Wasser und wassergesättigter Luft). Holz Roh- Werkst 21:19–22. https://doi.org/10.1007/BF02605991

Perkitny T, Lawniczak M, Marciniak H (1959) The influence of steaming on the swelling pressure of wood (Über den Einfluß des Dämpfens auf den Quellungsdruck des Holzes). Holz Roh- Werkst 17:54–61. https://doi.org/10.1007/BF02626322

Peura M, Andersson S, Salmi A et al (2008) Changes in nanostructure of wood cell wall during deformation. Mater Sci Forum 599:126–136. https://doi.org/10.4028/www.scientific.net/MSF.599.126

Popper R, Niemz P, Torres M (2006) Influence of the extractives of selected extraneous woods on the equilibrium moisture content (Einfluss des Extraktstoffanteils ausgewählter fremdländischer Holzarten auf deren Gleichgewichtsfeuchte). Holz Roh- Werkst 64:491–496. https://doi.org/10.1007/s00107-006-0132-x

Raczkowski J (1962) The swelling pressure of wood exerted by parts of a sample—part I: the partial sleeper swelling pressure (Über den durch Teile eines Probekörpers ausgeübter Quellungsdruck—Erste Mitteilung: Der Schwellen-Quellungsdruck). Holz Roh- Werkst 20:185–188. https://doi.org/10.1007/BF02604754

Raczkowski J (1970) The swelling pressure of wood exerted by sample parts—Part II: square bearing-plate swelling pressure (Über den durch Teile eines Probekörpers ausgeübten Quellungsdruck—Zweite Mitteilung: Der Stempel-Quellungsdruck). Holz Roh- Werkst 28:292–295. https://doi.org/10.1007/BF02615854

Ritger PL, Peppas NA (1987) A simple equation for description of solute release I. Fickian and non-fickian release from non-swellable devices in the form of slabs, spheres, cylinders or discs. J Controlled Release 5:23–36. https://doi.org/10.1016/0168-3659(87)90034-4

Roloff A, Grundmann BM (2008) Forest tree species and their use in climate change (Waldbaumarten und ihre Verwendung im Klimawandel). Arch Für Forstwirtsch Landschaftsökologie 42:97–109

Rybarczyk W, Ganowicz R (1974) A theoretical description of the swelling pressure of wood. Wood Sci Technol 8:233–241. https://doi.org/10.1007/BF00352027

Sánchez-Ferrer A, Engelhardt M, Richter K (2023) Anisotropic wood–water interactions determined by gravimetric vapor sorption experiments. Cellulose 30:3869–3885. https://doi.org/10.1007/s10570-023-05093-z

Schlotzhauer P, Nelis PA, Bollmus S et al (2017) Effect of size and geometry on strength values and MOE of selected hardwood species. Wood Mater Sci Eng 12:149–157. https://doi.org/10.1080/17480272.2015.1073175

Schwab E, Krause HA, Liesebach M, Stephan BR (2000) Wood properties of the Japanese Betula platyphylla var. japonica from a site in Northern Germany (Holzeigenschaften der Betula platyphylla var. japonica von einem norddeutschen Standort). Holz Roh- Werkst 58:184–190. https://doi.org/10.1007/s001070050411

Senalik CA, Farber B (2021) mechanical properties of wood. In: Wood handbook: wood as an engineering material. U.S. Department of Agriculture, Forest Service, Forest Products Laboratory, Madison, WI, USA

Shi SQ, Gardner DJ (2001) Dynamic adhesive wettability of wood. Wood Fiber Sci 33:58–68

Simo-Tagne M, Bennamoun L, Léonard A, Rogaume Y (2019) Determination and modeling of the isotherms of adsorption/desorption and thermodynamic properties of obeche and lotofa using nelson's sorption model. Heat Mass Transf 55:2185–2197. https://doi.org/10.1007/s00231-019-02577-2

Sing KSW, Everett DH, Haul RAW et al (1985) Reporting physisorption data for gas/solid systems with special reference to the determination of surface area and porosity (Recommendations 1984). Pure Appl Chem 57:603–619. https://doi.org/10.1351/pac198557040603

Skaar C (1988) Wood-water relations. Springer, Berlin

Stamm AJ (1959) Bound-water diffusion into wood in the fiber direction. For Prod J 9:27–32

Thybring EE, Glass SV, Zelinka SL (2019) Kinetics of water vapor sorption in wood cell walls: state of the art and research needs. Forests 10:704. https://doi.org/10.3390/f10080704

Tshabalala MA (1997) Determination of the acid-base characteristics of lignocellulosic surfaces by inverse gas chromatography. J Appl Polym Sci 65:1013–1020. https://doi.org/10.1002/(SICI)1097-4628(19970801)65:5%3c1013::AID-APP19%3e3.0.CO;2-2

Viljanen M, Ahvenainen P, Penttilä P et al (2020) Ultrastructural X-ray scattering studies of tropical and temperate hardwoods used as tonewoods. IAWA J 41:301–319. https://doi.org/10.1163/22941932-bja10010

Viollaz PE, Rovedo CO (1999) Equilibrium sorption isotherms and thermodynamic properties of starch and gluten. J Food Eng 40:287–292. https://doi.org/10.1016/S0260-8774(99)00066-7

Wadsö L (1994) Describing non-Fickian water-vapour sorption in wood. J Mater Sci 29:2367–2372. https://doi.org/10.1007/BF00363428

Walinder MEP, Gardner JD (2000) Surface energy of extracted and non-extracted Norway sprucewood particles studied by inverse gas chromatography (IGC). Wood Fiber Sci 32:478–488

Wangaard FF, Granados LA (1967) The effect of extractives on water-vapor sorption by wood. Wood Sci Technol 1:253–277. https://doi.org/10.1007/BF00349758

Willems W (2014) The water vapor sorption mechanism and its hysteresis in wood: the water/void mixture postulate. Wood Sci Technol 48:499–518. https://doi.org/10.1007/s00226-014-0617-4

Willems W (2015) A critical review of the multilayer sorption models and comparison with the sorption site occupancy (SSO) model for wood moisture sorption isotherm analysis. Holzforschung 69:67–75. https://doi.org/10.1515/hf-2014-0069

Willems W (2020) Effects of latent heat exchange on water vapor sorption kinetics. In: Proceedings of the 63rd international convention of society of wood science and technology. Portoroz, Slovenia

Zabler S, Paris O, Burgert I, Fratzl P (2010) Moisture changes in the plant cell wall force cellulose crystallites to deform. J Struct Biol 171:133–141. https://doi.org/10.1016/j.jsb.2010.04.013

Zhou H, Xu R, Ma E (2016) Effects of removal of chemical components on moisture adsorption by wood. BioResources 11:3110–3122. https://doi.org/10.15376/biores.11.2.3110-3122